The Meteoritical Society

Meteoritics & Planetary Science 57, Nr 9, 1745–1758 (2022)
doi: 10.1111/maps.13898

Geochemical evidence for the origin of the IIE parent body from H chondrite-like material

S. N. TEPLYAKOVA [1]*, M. HUMAYUN [2], C. A. LORENZ [1], and M. A. IVANOVA [1]

[1]Vernadsky Institute of Geochemistry and Analytical Chemistry, Russian Academy of Sciences, Kosygina st. 19, 119991 Moscow, Russia
[2]National High Magnetic Field Laboratory and Department of Earth, Ocean & Atmospheric Science, Florida State University, 1800 E. Paul Dirac Drive, Tallahassee, Florida 32310, USA
*Corresponding author. E-mail: elga.meteorite@gmail.com

(Received 21 February 2022; revision accepted 28 June 2022)

Abstract–Isotopic compositions of O, Mo, and Cu in the IIE iron meteorites have indicated a close affinity to the H chondrite group. The diversity of trace element compositions and their abundance of silicate inclusions indicate that IIE iron meteorites were formed in multistage processes. To better constrain the formation of the IIE irons, this study analyzed elemental abundances in the metal of five IIE irons (Elga, Miles, Tobychan, Verkhne Dnieprovsk, and Watson) by laser ablation inductively coupled plasma mass spectrometry. The data are interpreted in terms of a new model of IIE crystallization from the metal fraction of completely molten H chondrite-like material based on the solid/liquid distribution coefficients of siderophile and chalcophile elements changing simultaneously with changes of S concentrations in the remaining liquid during the crystallization of the Fe,Ni phase in the Fe-Ni-S system. The model showed that IIE iron compositions could be produced as solid phases at 40–73 wt% of fractional crystallization of the metal component of a bulk H chondrite-like metallic melt. We propose that IIE iron metal could have originated from the solidified core of a differentiated body of H chondrite-like composition and sampled different fractions of that core exposed during a catastrophic disruption of the body. The present structure of metal and silicate inclusions of IIE irons was formed by remelting and metal–silicate mixing during late impact event(s) on the parent body surface.

INTRODUCTION

Iron meteorites have a notable diversity of chemical groups, indicating that they come from multiple parent bodies. Some parent bodies could be the fragments of asteroid cores that experienced melting and magmatic differentiation shortly after accretion of planetesimals (Markowski et al., 2006; Qin et al., 2008; Scherstén et al., 2006; Snyder et al., 2001). Melting was caused by internal radiogenic heat sources (Qin et al., 2008; Schulz et al., 2009, 2012). These asteroids could be partially or completely differentiated (McCoy, 1995; Prinz et al., 1980; Wasserburg et al., 1968). Magmatic iron meteorites formed inside asteroids during fractional crystallization of the core. They include the IIAB, IIIAB, IVA, IVB, IC, IIC, IID, IIIE, IIF, and IIIF groups (Mittlefehldt et al., 1998). Nonmagmatic groups of iron meteorites are believed to have formed through large-scale collisions of asteroids, followed by the segregation of a pool of melt containing metal and silicate components (Bild & Wasson, 1977; Casanova et al., 1995; Ebihara et al., 1997; Ikeda & Prinz, 1996; Ikeda et al., 1997; Mittlefehldt et al., 1998; Olsen et al., 1994; Osadchii et al., 1981; Scott & Wasson, 1976). Genetic relationships of iron meteorites with meteorites of other types are not always clear, with the exception of isotopic proximity (Burkhardt et al., 2011; Clayton & Mayeda, 1996; Kruijer & Kleine, 2019).

Group IIE iron meteorites have features of both magmatic and nonmagmatic meteorites and members of the NC group in Mo isotopes (Kruijer & Kleine, 2019). Only 22 iron meteorites of group IIE are known

(Meteoritical Bulletin Database, 2022). IIE iron meteorites have similar metal chemical composition (Ni, 8.27 ± 0.54 wt%; Ga, 23.9 ± 3.04 μg g^{-1}; Ge, 88.3 ± 78.0 μg g^{-1}; Ir, 5.02 ±1.6 μg g^{-1}) and also contain varying amounts of silicate inclusions with compositions ranging from undifferentiated to highly differentiated (Ruzicka & Hutson, 2010; Scott & Wasson, 1976; Wasson, 2017; Wasson & Wang, 1986). Group IIE meteorites are also characterized by having only small variations in Ir content in the metal (1.12–7.95 μg g^{-1}; Wasson, 2017), compared to meteorites of other magmatic groups in which Ir concentrations vary in a wide range and by a factor of 6000 within the group. For example, group IIAB meteorites contain from 0.01 to 60 μg g^{-1} Ir (Wasson, 2017).

IIE irons have a link to H chondrites in the oxygen isotope compositions of their silicate inclusions (Clayton & Mayeda, 1996). A new high-precision laser fluorination study of the oxygen isotopic composition of IIE silicates reveals almost complete overlap with the equilibrated H chondrites (McDermott et al., 2016). Isotopic compositions of Cu and Mo of the metal of IIE meteorites are also close to H chondrites (Bishop et al., 2012; Burkhardt et al., 2011; McDermott et al., 2016).

IIE irons have been linked to the asteroid 6 Hebe by reflectance spectra that could indicate the presence of metal sheets on its surface (Gaffey & Gilbert, 1998). Endogenic models of the genesis of IIE iron meteorites involve the interior heating of asteroids together with complete separation of metal and sulfide from silicate as the main formation process (Kruijer & Kleine, 2019; McCoy, 1995; Teplyakova et al., 2012, 2018; Wasserburg et al., 1968). Recent results based on W and Pt isotopic data (Kruijer & Kleine, 2019) are consistent with a single partial metal–silicate differentiation event driven by endogenic heating at ~4–5 Ma after calcium–aluminum-rich inclusion (CAI) formation, followed by one or multiple impact events resulting in mixing and re-equilibration of metal and silicates in later stages of formation. A recent paleomagnetic investigation by Maurel et al. (2021) indicated that the cores of the IIE parent bodies generated dynamo magnetic fields from 80 to 160 Ma years after CAI formation.

However, the link between IIE meteorites and H chondrites has been questioned due to differences in the trends of Ga-Au and Ir-Au in the IIE metal and H chondrite metal (Wasson & Scott, 2011; Wasson & Wang, 1986). Silicates in IIE meteorites are more magnesian than in H chondrites. Based on these facts, Wasson (2017) suggested that "IIE meteorites were produced by impacts onto an HH asteroid with composition similar to Netschaevo." However, the concept of an LL-L-H-HH metal–silicate differentiation trend in ordinary chondrites (Russell et al., 1998) was not supported by Troiano et al. (2011), who proposed a common origin for the low-FeO chondrites Burnwell, EET 96010, and LAP 04757, and the H chondrites based on oxygen isotopes and trace element compositions. A recent investigation (Rubin, 2022) showed that meteorites of the IIE-H-L-LL trend have mineralogical, chemical, isotopic, and physical similarities.

In addition, variations in mass-dependent fractionation of Ge isotopic compositions detected in the metal of IIE meteorites have been explained by evaporation with the loss of light isotopes of Ge and Ga (Luais, 2007) from the surface of the parent body, probably due to a shock event. Based on these facts, some researchers concluded that the metal of IIE irons was formed at the surface of the parent asteroid in the form of layers of metallic melt segregated from chondritic impact melt (Ebihara et al., 1997; Scott & Wasson, 1976; Wasson, 2017; Wasson & Scott, 2011; Wasson & Wang, 1986), rather than crystallizing in the asteroid core during fractional crystallization of the metallic melt. This interpretation is supported by the medium-grained metal structure of IIE meteorites in which the size of γ-iron crystals (1–11 cm) is small compared to the meter-sized (up to 2 m) crystals in IIIAB meteorites (Wasson, 2017). However, correlations which were found for two pairs of compatible and incompatible elements: Ga-Au and Ir-Au (Wasson, 2017), along with a positive correlation of Au and As (correlation coefficient of $R^2 \sim 1$), are characteristics of magmatic meteorites (Scott & Wasson, 1976; Wasson, 2017; Wasson & Wang, 1986).

IIE meteorites contain silicate inclusions of chondritic composition in Netschaevo and Watson, and highly fractionated silica-, alkali-rich silicate inclusions in Colomera, Miles, and Elga (Olsen et al., 1994; Ruzicka et al., 1999; Ruzicka & Hutson, 2010; Teplyakova et al., 2018; Wasserburg et al., 1968). The formation and coexistence of silicate inclusions with the metal in IIE irons are difficult to explain, considering the endogenous conditions of asteroids, and likely may be connected with late reprocessing of the IIEs' parent bodies (Kruijer & Kleine, 2019; Rubin, 2022; Ruzicka, 2014; Teplyakova et al., 2018). However, despite the progress described above, modeling of the IIE metal from H chondrite-like material has not yet been performed. The main purpose of this article is to explore the primary processes of IIE iron formation through the investigation of siderophile element distribution in the metal of IIE irons and the modeling of fractional crystallization of the H chondrite-like metallic melt as a possible precursor of IIE irons.

SAMPLES AND ANALYTICAL PROCEDURES

Polished sections of the IIE iron meteorites Elga, Miles, Tobychan, Verkhne Dnieprovsk, and Watson provided by the Meteorite collection of the Russian Academy of Sciences were studied by optical microscopy in reflected light (Leica DMRX) at the Vernadsky Institute of Geochemistry and Analytical Chemistry. Major and trace element compositions of metal and sulfide phases were determined by laser ablation inductively coupled plasma mass spectrometry (LA-ICP-MS) following procedures described previously (Campbell & Humayun, 1999; Humayun, 2012) at Florida State University, USA. The laser ablation system utilized was a New Wave UP 193FX 193 nm ArF excimer laser coupled to a Thermo Element XR single collector, magnetic sector ICP-MS. Bulk chemical compositions were analyzed by laser tracks (50 μm spot, scanned at 10 μm s^{-1}). Rasters with 100 μm spot size scanned at 25–50 μm s^{-1} were performed on areas ranging from 0.5 to 4 mm to average over the areas of the prominent Widmanstätten structure. A 20 Hz pulsed laser beam was scanned over the surface of each sample at rate of 10 μm s^{-1} by monitoring the isotopes: ^{29}Si, ^{31}P, ^{34}S, ^{51}V, ^{53}Cr, ^{55}Mn, ^{57}Fe, ^{59}Co, ^{60}Ni, ^{63}Cu, ^{66}Zn, ^{69}Ga, ^{74}Ge, ^{75}As, ^{82}Se, ^{83}Kr, ^{93}Nb, ^{97}Mo, ^{102}Ru, ^{103}Rh, ^{106}Pd, ^{107}Ag, ^{109}Ag, ^{111}Cd, ^{115}In, ^{120}Sn, ^{121}Sb, ^{125}Te, ^{184}W, ^{185}Re, ^{192}Os, ^{193}Ir, ^{195}Pt, ^{197}Au, ^{205}Tl, ^{208}Pb, ^{209}Bi. Standards used in this study included Hoba IVB (Ru, Rh, Pd, Re, Os, Ir, Pt; Walker et al., 2008), Filomena IIA (Cu, Ga, Ge, As, W, Au; Wasson et al., 1989), NIST SRM 1263a (V, Cr, Cu, As, Mo, Ag, W, Au; Campbell et al., 2002), and NIST SRM 610 (Si, P, S, Se, Nb, Ag, Cd, In, Sn, Sb, Te, Tl, Pb, Bi; Gaboardi & Humayun, 2009; Jochum et al., 2006). Each line scan was a few millimeters in length; the reported data are averages of several such line scans. Uncertainties of analyses include error of these averages in addition to variation in repeated measurements of the standards.

RESULTS

Characteristics of Analyzed Samples of IIE Irons

Similar to most IIE iron meteorites, the metal of the five studied meteorites (Elga, Miles, Tobychan, Verkhne Dnieprovsk, and Watson) is represented by nickel–iron, which is an aggregate of low-Ni α-Fe ("kamacite") and taenite (γ-Fe) with minor amounts of schreibersite and troilite. These meteorites have a polycrystalline structure of polygonal grains ~1–6 cm across (Teplyakova & Lorenz, 2019). Each individual taenite grain shows an octahedrite inner structure, which is defined by kamacite lamellae and schreibersite crystals co-oriented in parallel to the octahedron faces in taenite. Miles consists mainly of kamacite with rare taenite and schreibersite inclusions. Rounded and amoeboid silicate inclusions (in Elga, Miles, and Watson), troilite nodules (see Fig. 2b), and large anhedral schreibersite grains aligned along the boundaries of taenite crystals and rims around silicate inclusions are similar for all studied meteorites. In Elga, Miles, Tobychan, Verkhne Dnieprovsk, and Watson, we observed (Teplyakova & Lorenz, 2019) that schreibersite was more abundant than in previously reported IIE meteorites (Olsen et al., 1994; Van Roosbroek et al., 2017). The higher content of phosphorus could play a role in forming magmatic and metamorphic structures in the metal and in the distribution of siderophile trace elements during fractional crystallization (Corrigan et al., 2009; Teplyakova & Lorenz, 2019).

In Elga, Tobychan, Verkhne Dnieprovsk, and Watson, local zones of quenched Fe-Ni-P-S melts were observed (Bevan et al., 1979; Buchwald & Clarke, 1987; Khisina et al., 2017, 2019; Litasov et al., 2019; Olsen et al., 1994; Osadchii et al., 1981). In Elga, Fe-Ni-P-S-C-O melt pockets have unusual composition (Khisina et al., 2017, 2019) and could be formed at higher pressure near 20 GPa (Litasov et al., 2019). In the Miles and Tobychan sections studied, melt pockets are absent. Tobychan contains unusual rose-like structures in kamacite, which could have formed during a shock event (Buchwald, 1976).

Distribution of Siderophile Trace Elements in the Metal of IIE Iron Meteorites

Siderophile element compositions of the metal of Verkhne Dnieprovsk, Tobychan, Elga, Miles, and Watson are presented in Table 1 and shown in an Fe-, CI-normalized plot in comparison with the literature data in Fig. 1. These data are mostly comparable with those obtained previously for IIE iron meteorites by instrumental neutron activation analysis (INAA; Ebihara et al., 1997; Scott et al., 1973; Wasson, 2017; Wasson & Scott, 2011; Wasson & Wang, 1986) (Fig. 1).

The relative deviations of values for the Elga meteorite obtained by LA-ICP-MS are about 10% higher for Ni, Co, Re, Ga, Ge, and Au and 15–20% higher for Cu, Ir in comparison to values obtained recently by the INAA method. For Tobychan, the average values of two samples have a deviation of Ir and Re concentrations ~25% higher and deviation of Ni~15% lower than previously reported (Wasson, 2017). For other elements, the relative deviation does not exceed 6%.

Table 1. Bulk composition (μg g^{-1}) and their standard deviations (σ) of 24 elements in the metal of five IIE irons: Verkhne Dnieprovsk, Tobychan, Elga, Miles, and Watson by LA-ICP-MS analysis.

	Model metal liquid	Verkhne Dnieprovsk		Tobychan		Elga		Miles		Watson	
V*	—	4		130		58		192		64	
		Average	σ	Average	σ	Average	σ	Average	σ	Average	σ
Si		120	33.15	145	154	115	11	368	36	322	152
P	4623	677	121	895	128	5282	2026	3432	3320	7167	1502
S	85,623	488	214	221	192	190	65	129	101	430	134
Cr		19.81	7.63	3.42	1.37	12.75	2.25	4.46	0.28	19.74	1.40
Fe	831,201	917,385	12,264	927,332	4645	913,274	3433	910,196	10,833	900,795	3677
Co	3467	4849	196	4376	47.29	4316	37	4269	131	4493	115
Ni	74,492	76,126	12,043	66,687	4594	76,507	1477	81,268	8209	86,461	2816
Cu	428	169	57	167	25	153	5.32	191	29	166	8
Zn		2.88	2.23	6.44	9.45	2.52	1.31	2.36	0.69	4.73	1.36
Ga	25.7	24.24	5.80	29.46	1.69	22.34	0.63	28.21	1.51	21.82	0.78
Ge	55.7	74.82	10.56	70.73	2.79	67.60	1.19	71.17	1.87	52.50	1.74
As	8.78	8.68	1.28	7.33	1.29	9.58	0.55	6.48	1.00	9.41	0.97
Mo	7.28	6.74	1.61	5.63	0.16	7.62	0.54	6.11	1.23	8.16	0.48
Ru	5.60	8.49	1.68	9.64	0.46	8.13	0.15	6.36	0.37	9.67	0.26
Rh	1.21	1.45	0.26	1.45	0.06	1.37	0.03	1.26	0.04	1.50	0.03
Pd	4.38	3.65	0.88	2.93	0.31	3.63	0.09	3.52	0.22	4.32	0.16
Sn	3.68	1.25	0.75	0.72	0.07	0.83	0.03	0.66	0.06	0.22	0.03
Sb	0.30	0.32	0.28	0.12	0.02	0.15	0.00	0.11	0.02	0.23	0.04
W	0.68	1.28	0.18	1.34	0.06	1.22	0.01	0.80	0.02	1.20	0.05
Re	0.38	0.59	0.05	0.85	0.03	0.48	0.01	0.15	0.01	0.70	0.04
Os	4.13	8.75	1.57	10.03	0.38	5.08	0.09	1.29	0.08	8.60	0.44
Ir	3.63	7.00	1.14	8.46	0.23	4.89	0.08	1.55	0.06	6.73	0.27
Pt	7.79	11.86	1.68	13.45	1.07	11.24	0.19	6.92	0.16	11.88	0.40
Au	1.21	1.39	0.25	0.87	0.10	1.19	0.03	0.92	0.06	1.17	0.08
W	1.69	2.87	0.44	2.96	0.13	2.75	0.03	1.80	0.03	2.75	0.13
Re	2.36	3.37	0.29	4.79	0.15	2.75	0.06	0.84	0.04	4.04	0.21
Os	1.95	3.74	0.72	4.24	0.15	2.18	0.04	0.56	0.03	3.74	0.19
Ir	1.73	3.02	0.53	3.61	0.09	2.12	0.03	0.67	0.03	2.96	0.12
Ru	1.80	2.48	0.53	2.78	0.15	2.38	0.04	1.87	0.13	2.87	0.08
Pt	1.80	2.49	0.38	2.79	0.22	2.37	0.04	1.46	0.03	2.54	0.09
Rh	2.07	2.25	0.43	2.22	0.10	2.14	0.04	1.97	0.07	2.36	0.04
Mo	1.80	1.51	0.38	1.24	0.04	1.71	0.13	1.38	0.30	1.86	0.11
Ni	1.55	1.44	0.25	1.25	0.09	1.45	0.03	1.55	0.18	1.66	0.06
Co	1.58	2.01	0.08	1.79	0.02	1.79	0.01	1.78	0.04	1.89	0.05
Pd	1.79	1.36	0.35	1.08	0.12	1.35	0.03	1.31	0.09	1.63	0.06
Fe	1.00	1.00	0.00	1.00	0.00	1.00	0.00	1.00	0.00	1.00	0.00
Au	1.98	2.07	0.40	1.28	0.15	1.77	0.05	1.37	0.10	1.77	0.12
As	1.08	0.97	0.15	0.81	0.14	1.07	0.06	0.73	0.11	1.07	0.11
Sb	0.48	0.47	0.43	0.18	0.03	0.23	0.00	0.17	0.04	0.35	0.06
Cu	0.78	0.28	0.10	0.27	0.04	0.25	0.01	0.32	0.05	0.28	0.01
Ga	0.59	0.50	0.13	0.61	0.04	0.47	0.01	0.59	0.03	0.46	0.02
Ge	0.39	0.48	0.07	0.44	0.02	0.43	0.01	0.46	0.01	0.34	0.01
Sn	0.36	0.15	0.09	0.09	0.01	0.10	0.00	0.08	0.01	0.03	0.00

*V—volume of the evaporated substance by the laser in microns.[3]

For Miles metal, the LA-ICP-MS data coincide with the INAA data (relative deviations ≤ 7% for all elements). For Rh, Pd, and Au, the deviation is 20% higher; for As and Sn, it is 30–40% lower; and for Ru, Re, and Ir, it is 50–70% higher than previously shown (Ebihara et al., 1997; Wasson, 2017). Os abundance (1.29 ppm) is in good agreement with Scott et al. (1973; 1.24 ppm), and Pt abundance (7.06 ppm) is confirmed by our results (6.92 ppm). However, Sb (0.11 ppm) is similar to that obtained by Wasson and Wang (1986)

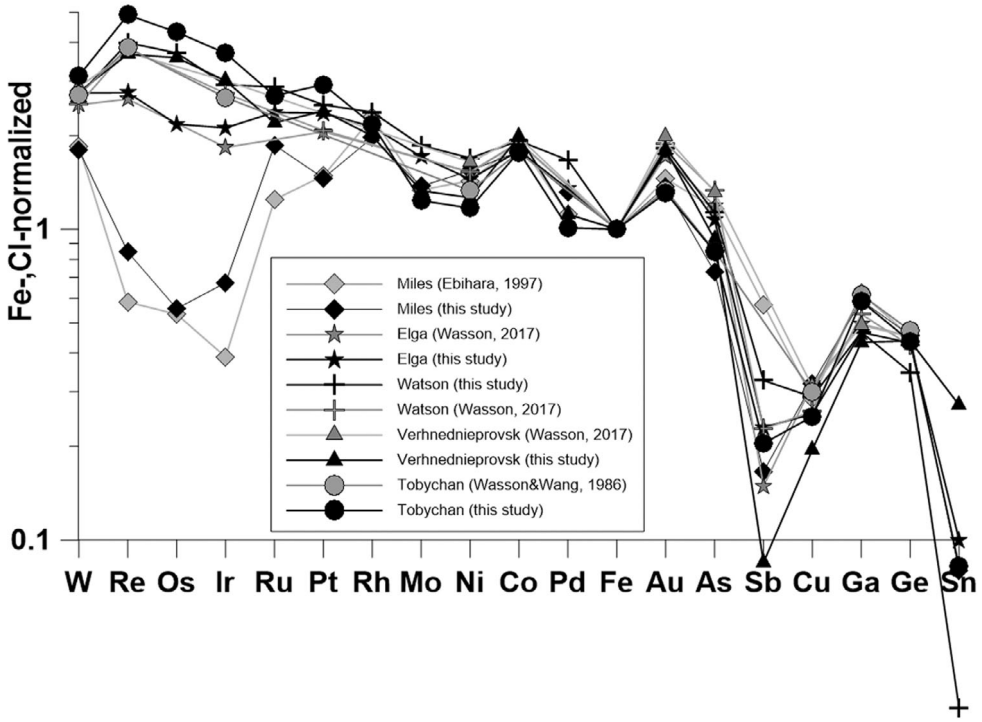

Fig. 1. The distribution of siderophile elements in IIE irons according to LA-ICP-MS data compared with published data obtained by INAA (Wasson, 2017; Wasson & Wang, 1986) normalized to Fe-, CI-chondrites (Anders & Grevesse, 1989). For Verkhne Dnieprovsk, Sb < 0.1; for other IIE irons, beside Verkhne Dnieprovsk, Sn < 0.1.

and Wasson and Scott (2011), but four times lower than the Sb content of Scott et al. (1973). Since Au and As prefer to distribute in taenite and kamacite, respectively, our higher $(Au/As)_{CI}$ ratio for Miles (1.9) indicates that we have samples with more abundant taenite than samples analyzed by INAA in which the $(Au/As)_{CI}$ ratio is 1.3 (Scott et al., 1973) and 1.6 (Wasson & Wang, 1986). The Verkhne Dnieprovsk sample was only a few millimeters in size and highly oxidized, and the metal area available for the raster LA-ICP-MS analysis was much lower than for the other IIE iron meteorites in this study. Three spot analyses were also performed. Abundances for these spots are in good agreement with the INAA data (Fig. 1), except for As, which is 60% lower than obtained by INAA (Wasson & Wang, 1986), possibly due to an unrepresentative sample with partially oxidized (As-bearing) kamacite.

Siderophile element compositions of four studied IIE iron meteorites show enrichment in refractory elements, while the Miles composition is depleted in refractory element Ga and depleted in incompatible elements—Pd, Au, As, and partially Sb, Cu, and Sn in comparison with the metal of H chondrites (Kong & Ebihara, 1997). The metal of IIE irons is similar in composition to the metal of H chondrites by the elements with distribution coefficient between the solid metal and the liquid metal ($D_{sol/liq}$) ~1 (Kong & Ebihara, 1997), such as Ni, Co, Ge, and Pd, Au, As.

The Ga-Au and Ir-Au correlations in the studied IIE iron meteorites are poorly defined (Fig. 2a), which is not consistent with the crystallization trends of the magmatic iron meteorites. At the same time, these IIE meteorites are characterized by a positive correlation of the incompatible siderophile elements Au and As (Fig. 2b) and compatible elements Os and Ir (correlation coefficient $R^2 \sim 1$; Fig. 2b and 2c). The W/Ni-Fe/Ni CI-normalized ratios of the IIE irons metal are well correlated (Fig. 2d), which differ from that of the bulk metal from H3 chondrites (Kong & Ebihara, 1997) and the bulk H, L, and LL chondrite compositions (Wasson & Kallemeyn, 1988). The distribution patterns of the refractory siderophile elements and gallium are compatible with the solid metal phase in Tobychan, Elga, Verkhne Dnieprovsk, and Watson meteorites (Figs. 1 and 3), and plot above the line of the equilibrated H chondrite metal.

DISCUSSION

As was noted above, the incompatible elements Au and As are usually well correlated during melting and fractional crystallization processes. Figure 2b shows a

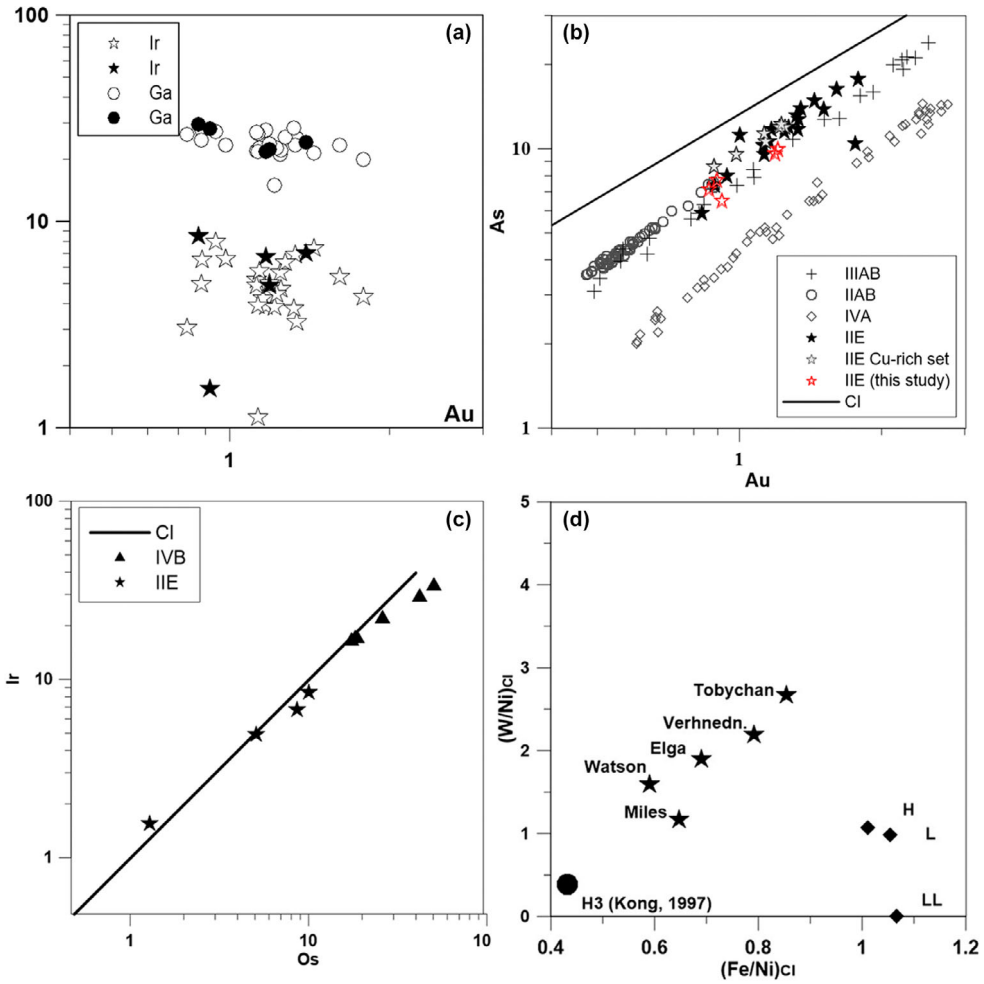

Fig. 2. a) Correlations of Au-Ga, black circles (this study), white circles (Wasson, 2017), Au-Ir, black stars (this study), and white stars (Wasson, 2017). b) Positive magmatic correlations of Au-As in meteorites of groups IIAB (Wasson et al., 2007), IIIAB (Wasson, 1999), IVAB (Wasson & Richardson, 2001), IIE irons, red open stars (this study), black filled stars (Wasson, 2017), and gray filled stars (Cu-rich set; Wasson, 2017). c) Positive correlation of Os-Ir in meteorites of groups IVB (Campbell & Humayun, 2005) and IIE irons, black stars (this study). d) $(W/Ni)_{CI}$—$(Fe/Ni)_{CI}$ chondrite normalized ratio for the bulk metal from H3 chondrites (Kong & Ebihara, 1997); the bulk H, L, and LL chondrite compositions (Wasson & Kallemayn, 1988); the bulk rasters from IIE irons. (Color figure can be viewed at wileyonlinelibrary.com.)

plot of Au versus As for IIE iron meteorites in comparison with those for magmatic IIAB, IIIAB, IVA iron meteorites. IIE and other irons, except for IVA iron meteorites, form coherent trends. None of these iron meteorite groups plot along the CI trend. Analyses of IIE irons plot along the trend defined by IIAB–IIIAB, which is distinct from the IVA iron meteorite trend that was probably formed by some volatile loss processes that occurred on the IVA parent body (McCoy, 2011; Wasson & Richardson, 2001).

The ratios of Re/Os, Re/Ir in the IIE irons indicate fractionation similar to that observed in the magmatic iron meteorite groups (Fig. 2c). Fractionation of Os from other elements of the platinum group is not a characteristic of the condensation of material in the protoplanetary disk (Campbell et al., 2002). The Os/Ir ratio in IIE irons is not chondritic and, hence, likely to be a consequence of the fractional crystallization of solid metal from metallic melt. Since both Os and Ir are compatible with the solid phase, but Os is preferentially distributed into solid metal ($D_{Os} > D_{Ir}$, where D is the solid metal/liquid metal distribution coefficient; Chabot et al., 2003), the positive linear trend for the Os/Ir ratio has a smaller slope compared to this trend in chondrites, where the ratio Os/Ir is ~1 (Anders & Grevesse, 1989; Campbell et al., 2002). The IIE and IVB iron meteorites have $(Ir/Os)_{CI} \sim 0.8–1.3$ and 0.9–2.5, respectively.

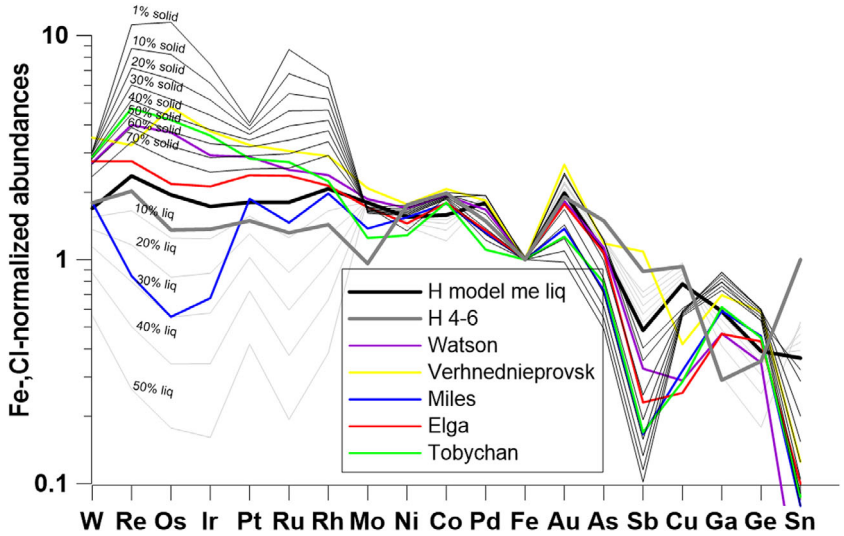

Fig. 3. Model compositions of the liquid metal (gray lines) and the solid metal (black lines) formed during fractional crystallization of the H chondrite model metal liquid (dashed black line) in comparison with IIE meteorites and the total metal composition of equilibrium H4-6 chondrites (Kong & Ebihara, 1997). (%)—the proportion of crystals or residual liquid normalized to Fe, CI (Anders & Grevesse, 1989). (Color figure can be viewed at wileyonlinelibrary.com.)

Thus, the Au/As and Os/Ir ratios of the studied IIE iron meteorites correspond better to the fractional crystallization of a metallic melt of an H chondrite-like precursor. Siderophile element distribution indicates that the IIE metal is more reduced than the H chondrite metal (Teplyakova et al., 2012; Wasson & Scott, 2011; Wasson & Wang, 1986). The $(W/Ni)_{CI}$ and $(Fe/Ni)_{CI}$ ratios in the investigated IIE meteorites (Fig. 2d) support these suggestions—IIE irons plot above metal from H chondrites, indicating a higher enrichment in W corresponding to more reduced conditions during IIE formation. The metal of IIE meteorites is significantly enriched in Ga in comparison with the metal of H chondrites (Fig. 3). Since Ga is more preferentially distributed in the solid fraction during fractional crystallization of Fe-Ni-S (P) melts (Chabot et al., 2003; Corrigan et al., 2009), the enrichment of Ga of the IIEs metal could be explained by self-reduction of the H chondrite-like precursor. The Ga distribution coefficient between metal and silicates ($D_{met/sil}$) depends on oxygen fugacity and varies from 88.4 at $fO_2 = 10^{-14}$ atm at 1300°C to 1.8 at $fO_2 = 10^{-10}$ at 1300°C and 48.5 at $fO_2 = 10^{-10}$ atm at 1600°C to 1.1 at $fO_2 = 10^{-8}$ at 1600°C (Schmitt et al., 1989).

Thus, the IIE metal could be formed from H chondrite material by its complete melting and reduction of W, Ga and other siderophile elements, segregation of the metallic liquid, and its fractional crystallization. Rubin (2022) suggested that IIE irons were derived from chondritic precursors that were the most reduced ordinary chondrites, probably from a composition close to "HH chondrites." However, our data showed that the IIE metal could be formed from H chondrite-like material by complete melting and reduction of W, Ga and other siderophile elements, segregation of the metallic liquid, and its fractional crystallization.

Model of IIE Irons' Origin from Completely Molten H Chondrite-Like Material

To test the hypothesis of a IIE metal origin from the H chondrite-like parent body, a model of fractional crystallization of the metal from a completely molten composition similar to H chondrites was constructed. The H chondrite-like bulk composition was compiled from average bulk compositions of chondrites by Wasson and Kallemayn (1988)—for W, Mo, Cu, Ge, Sb, Sn, Se, S, P; Jarosewich (1990)—for Fe and Ni; Fischer-Godde et al. (2010)—for Re, Os, Ir, Pt, Ru, Rh, Pd.

The composition of the S-bearing metal fraction of this H chondrite-like model liquid was calculated from the bulk composition of H chondrites (Jarosewich, 1990). Iron content in the metal liquid (Fe_{ml}) is calculated as the sum of metal iron (Fe_{met}), sulfide iron, and Ni abundances (wt%) taken from Jarosewich (1990) for average H chondrite falls and accepted as 100 wt% using the following equation:

$$Fe_{ml} = (Fe_{met} + 0.64FeS) \times 100\%/(Fe_{met} + Ni + FeS), \quad (1)$$

where 0.64 is the weight portion of iron in troilite. The inferred parental metallic liquid composition is presented in Table 1.

During fractional crystallization of the metallic melt, incompatible elements S, C, and P gradually accumulate in the residual liquid. While crystallization proceeds, the distribution coefficients of siderophile elements between the metal solid phases and liquid ($D_{sol/liq}$) are gradually changed (Jones & Drake, 1983; Willis & Goldstein, 1982). It was experimentally established that increase of sulfur concentration in the melt from 1 up to 31 wt% (Fe-FeS eutectic) resulted in an increase of *D*s of siderophile elements, for example, $D_{sol/liq}$ (Ge) increases from 0.6 to 120 (Jones & Malvin, 1990). In the Fe-Ni-P system with increasing phosphorus concentration from 3 to 10 wt%, the value of $D_{sol/liq}$ (Ge) changes less abruptly than sulfur, from 1.1 to 2.4 (Corrigan et al., 2009). In this case, when the distribution coefficients are not constant, the Rayleigh equation describing fractional crystallization at constant *D*s cannot be used to describe the behavior of the whole system and a finite difference calculation was employed below. Since the distribution coefficient ($D_{sol/liq}$) is expressed in terms of a power–law function of the composition of the liquid metal (Jones & Malvin, 1990) and crystallization of a multicomponent melt is as a stage of phase reactions determined by the equilibrium phase diagram Fe-P-S (Raghavan, 1988), it is possible to calculate the trace element content in the residual liquid C_{liq} and in the solid phase C_{sol} at each stage of crystallization according to the simple fractional crystallization and equations of mass balance:

$$C_{liq} = \frac{C_i}{F + D - F \cdot D} \quad (2)$$

$$C_{sol} = D \cdot C_{liq} \quad (3)$$

where C_i is the weight concentration of the initial melt, C_{sol} is the weight concentration of an element in the crystallized solid, C_{liq} is the weight concentration of an element in the metallic liquid remaining after crystallization, *F* is the fraction of the liquid metal melt, and *D* is the solid/liquid distribution coefficient (weight) of the trace element at each stage of crystallization.

Using calculated values of 8.5 wt% of S and 0.4 wt % of P for the initial metallic model liquid (Table 1), the model calculates the equilibrium between solid metal and liquid metal at different degrees of fractional crystallization, with a step of 0.1% crystallization using formalism by Chabot and Jones (2003), and constants D0 and β (Chabot et al., 2003, 2009) (Fig. 3). At the last stage of crystallization (73%) of the model, the composition of the liquid corresponds to a eutectic Fe-S melt and has the lowest platinum group element content (Fig. 3).

The effect of P abundance on the solid and liquid compositions for partition coefficients of siderophile elements should be taken into consideration (Corrigan et al., 2009). The elements Rh, Ru, W, and Mo showed phosphorophile tendencies. Arsenic, Au, Ga, Ge, Ir, Os, Pt, Re, and Sb show slightly increasing partition coefficients with increasing P-content of the metallic liquid. Cobalt, Cu, Pd, and Sn showed constant partition coefficients. However, the phosphorous content in the calculated model liquid is only 0.4 wt%, which does not significantly change partition coefficients during the crystallization process.

In Fig. 3, the compositions of batch equilibrium residual liquids calculated for fractional crystallization of the initial model liquid at 10% step are shown. The residual liquids are all enriched in the incompatible elements, Pd, Au, As, Sb, Cu, and Sn, and depleted in compatible elements, W, Re, Os, Ir, Pt, Ru, relative to the initial liquid composition. A complementary effect is noted in solid metal that is in equilibrium with each of these residual liquids (Fig. 3).

Application of the Crystallization Model to the IIE Irons

Figure 3 shows that since the residual liquids are depleted in refractory compatible elements during fractional crystallization, the late solid phase compositions are likewise lower in the compatible elements, W, Re, Os, Ir, Pt, Ru, relative to the composition of the first solid phase. The metal compositions of Tobychan, Elga, Watson, and Verkhne Dnieprovsk plot above the model H chondrite-like metallic liquid composition in the range of compatible siderophile elements, while the incompatible elements, Pd, Au, As, and particularly Sb, Cu and Sn, are depleted in IIE metal (including Miles) relative to the H chondrite-like metallic liquid. The compositions of Verkhne Dnieprovsk, Tobychan, Watson, Elga, and Miles are comparable to the compositions of the solid phase crystallizing at ~40, ~45, ~55, ~70, and ~73% fractional crystallization of the initial metal liquid, respectively, indicating that all five studied IIEs could be formed as solid metal precipitated from a metallic liquid segregated from the molten H chondrite source.

None of the IIE metal compositions obtained in this study are consistent with compositions of the unfractionated metal liquid quenched within cooler silicate clasts during an impact event as proposed by Wasson (2017).

Scenarios for IIE Iron Formation

Several hypotheses have been proposed for the origin of IIE irons, including endogenous, exogenous, and hybrid origins of the metal and silicate fractions. Endogenous models based on differentiation of metallic liquid in the core (McCoy, 1995; Wasserburg et al., 1968) can explain the magmatic trends of Au-As and Os-Ir, as well as the distribution of siderophile elements in the IIE meteorites. Based on this, the IIE irons were considered products of complete melting of a chondritic source with subsequent segregation of the metallic liquid and its fractional crystallization in the cores of the parent body (ies). However, these models were not able to explain the relatively high cooling rate of the metallic melt when meter-sized well-crystallized crystals were observed in IIAB (Wasson, 2017), together with the occurrence of glassy silicate inclusions and H chondrite fragments inside the metal.

The exogenous group of models implies fractionation of metallic liquid at the surface of an asteroid during impact melting of chondrite material (Ebihara et al., 1997; Scott & Wasson, 1976; Wasson, 2017; Wasson & Scott, 2011; Wasson & Wang, 1986). These models can explain the poorly defined correlations of Ga/Ni, Ga/Au, Ge/Ni, Ga/Au, Ir/Au in the IIE metal, together with small size of metallic crystals due to relatively high cooling rates of metallic liquid. Wasson (2017) proposed that the absence of appreciable Ir fractionation probably indicates that the melts crystallized too quickly to allow fractional crystallization.

The hybrid models (Benedix et al., 2000; Kruijer & Kleine, 2019; Ruzicka, 2014; Teplyakova et al., 2012, 2018) combine endogenous sources and exogenous processes (impact melting or/and reaccretion of the fragments) for explaining the mixing of metal and IIE silicates. The hybrid model by Ruzicka (2014) suggests that during the catastrophic destruction of a partially differentiated asteroid, the liquid metal of the core was mixed with primitive and evolved material of the H chondritic-like precursor. However, our investigation indicates that the metal of IIE meteorites is a product of fractional crystallization of a melt. None of the investigated IIE meteorites correspond to the unfractionated metallic liquid of H chondrite composition that should represent a liquid core.

Rubin (2022) has shown that the silicates in the IIE irons are more reduced than the silicates in equilibrated H chondrites proposing that the trend of metal–silicate fractionation in ordinary chondrite-like bodies is LL-L-H-IIE. We showed that metal compositions of the IIE iron meteorites studied match well with the products of fractional crystallization of a metallic melt of an H chondrite-like precursor with enrichment in W and Ga of IIE metal being the result of self-reduction during the melting of the H chondrite parent body.

Thus, we assume that the metal and the silicates of IIE iron meteorites originated from the same parent body where the metal is a result of fractional crystallization of the core, while the silicates were fractionated in different degrees and likely represent the different horizons of silicate shell of the parent body. Based on our previous (Teplyakova et al., 2018) and recent investigations, we present a new hybrid model of the origin of the IIE iron meteorites.

According to our model (Fig. 4), the parent body of IIE meteorites had a composition similar to the H chondrite composition. This was a relatively large asteroid (hundreds of km diameter) and partially differentiated. We propose that the IIE meteorites may have formed in a three-stage process. In Stage 1, an H chondritic body was affected by incomplete internal differentiation with the formation of a metal core and a silicate mantle with the preservation of the outer H chondrite layer. Due to inward cooling (see review in Abrahams & Nimmo, 2019), the asteroid core was fractionally crystallized and became zoned by the distribution of siderophile elements. Based on short-lived radionuclide chronometers, it has been proposed (Hunt et al., 2018; Kruijer & Kleine, 2019) that the IIE parent asteroids accreted within 1.5 Ma after CAIs and reached a radius of more than 60 km and were partially melted. This melting and partial differentiation are proposed to be due to internal heating by ^{26}Al decay. Such duration of the differentiation of the proposed parent body of IIE meteorites correlates with the ages of differentiated achondritic meteorites and corresponds to the generally assumed early differentiation of large asteroids in the solar system (Birck & Allègre, 1978; Srinivasan et al., 2006). The compositions of IIE irons reflect the middle and late stages of fractional crystallization of the metal liquid in the core.

In Stage 2, as a result of catastrophic collisions with other asteroids, the parent asteroid of the IIE meteorites lost significant mass, including a part of its core (Fig. 4a), and the broken metal core became exposed at the surface. The partially destroyed asteroid of IIE irons was covered by a layer of regolith due to re-accretion of debris onto the asteroid surface after the disruption and impact reworking of this material and the rest of the outer chondrite layer (Fig. 4a). This regolith was composed of chondritic material of the outer layer and silicate products of the H chondrite-like fractionation from the deeper layers of the IIE parent body.

Possibly at this stage, mixing of fractionated IIE irons and Cu-rich materials occurred. During fractional crystallization, Cu should accumulate in the residual sulfide-rich liquid, because the solid–liquid distribution

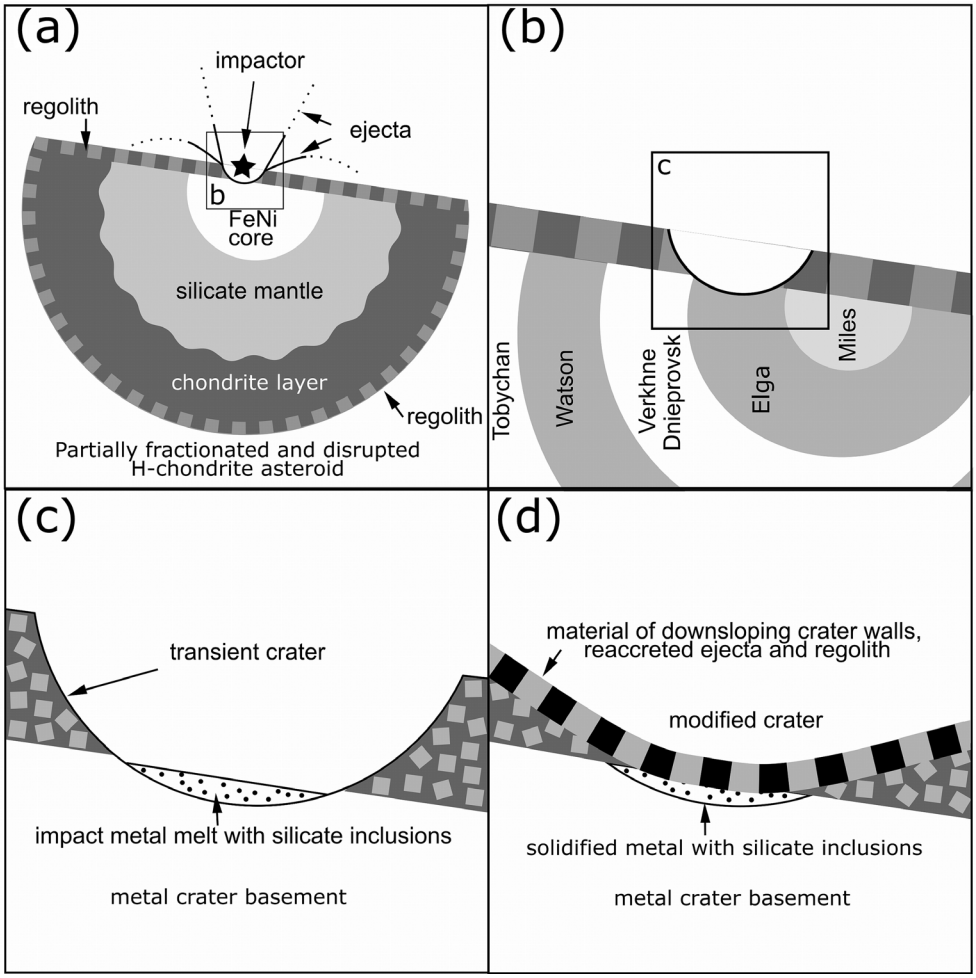

Fig. 4. A scheme of the scenario of the IIE irons' formation: (a) partially differentiated, destroyed parent body of IIE meteorites, consisting of (i) a metallic core and a silicate mantle, formed by complete melting of an H chondritic precursor; (ii) an outer undifferentiated H chondritic shell; (iii) and a surface regolith layer of predominantly chondritic composition which was formed by reaccretion of clasts ejected to the surface of a parent body after impact and postimpact reworking of this layer; star shows an impactor that formed the crater with a depth bigger than the thickness of the regolith layer; (b) zoned metallic core of the asteroid with outer and inner zones compositions of which correspond to IIE meteorites enriched or depleted in siderophile refractory elements, respectively; crater in metal with layers corresponding to those of the Elga metal; concentric zoning of the core of the IIE bodies is an oversimplified scheme of fractionally differentiated metal areas; (c) transient impact crater directly after formation; walls of the crater are composed mainly of regolith clasts, the area of impact metallic melt with inclusions of a silicate melt is localized at the floor of the impact crater; (d) modified crater with the floor covered by fragmented rocks formed by slumping of the transient crater walls and reaccretion of ejecta. Figure is modified after Teplyakova et al. (2018).

coefficient (D) of Cu is <1 (Chabot et al., 2009) for the FeS-rich metallic melt that is illustrated in our model. However, Cu-rich IIEs shown in Au-As diagram (Fig. 2b) plot among relatively Au-As-poor solids characteristic of the earlier stages of fractional crystallization. It is possible that (1) the contamination of residual trapped sulfide-rich Cu-bearing metal could have occurred during IIE remelting; or (2) mixing of exposed IIE metal with Cu-bearing metal of the outer, undifferentiated ordinary chondrite shell of the IIE parent body took place. As was suggested by Rubin (2022), the Cu-rich IIE irons likely formed from rapidly cooled impact melts near the surface of the IIE asteroid.

In Stage 3, the areas of the broken metal core of different regions were subsequently impacted melted and affected by evaporation of volatile elements such as Ga, Ge, and Au due to further impacts (Fig. 4a), but the fractionation features of the metal were retained. Meanwhile, the formation of the IIE irons within local impact melt sheets could explain the poorly defined correlations of Ga/Ni, Ga/Au, Ge/Ni, Ga/Au, Ir/Au in

the IIE metal. The similarity of structures of IIE metal shows that cooling was fast enough to form mm–cm size γ-Fe,Ni rimmed by schreibersite at ~1060–1100°C on the surface of the parent body (Teplyakova & Lorenz, 2019; Wasson, 2017). Metal shock melt was mixed with particles of silicate regolith in impact craters forming IIE irons with silicate inclusions (Fig. 4b and 4c). The localized melt pools inferred for IIEs also explain the Hf-W model age clusters of 4–5 million years (Ma), 10, 15, and 27 Ma after CAI formation (Kruijer & Kleine, 2019).

The diverse composition of IIE silicate inclusions could be the result of large-scale lateral inhomogeneity of the regolith that covered the metal target. At the initial stage of postimpact modification of the crater, the mixture of metal and silicate melts was cooled at relatively high cooling rates near the surface of the parent body, resulting in the formation of quenching structures of silicate inclusions (Teplyakova et al., 2018) and fine-grained polycrystalline metal structure (Teplyakova & Lorenz, 2019). Then, the impact melts were buried under the thermal insulating layer of regolith and the Widmanstätten patterns of individual taenite crystals in the Elga, Watson, Verkhne Dnieprovsk, and similar IIE meteorites were formed due to slower cooling (Fig. 4d). Rubin (2022) also showed that most IIE metal remained within the crust/mantle region alongside recrystallized chondritic clasts, that alkali-rich IIE silicate inclusions formed from late-stage impacts via preferential melting of plagioclase, and that some separation of K from Na occurred during vapor transport.

In Stage 4, the surface of the IIE parent body was affected by hypervelocity collisions with relatively small bodies, which resulted in the formation of melt pockets at temperatures of 1450°−1500°C and pressures above 20 GPa in Elga (Litasov et al., 2019) and possibly other meteorites: Watson, Verkhne Dnieprovsk (Bevan et al., 1979; Buchwald & Clarke, 1987), and Netschaevo (Van Roosbroek et al., 2017). Shock events also led to numerous cracks, shear deformations, and formation of Neumann lines in kamacite and, ultimately, to the separation and ejection of metal fragments from the surface of the parent body to Earth-crossing trajectories.

SUMMARY

We present clear geochemical evidence of a magmatic origin of the IIE meteorites Verkhne Dnieprovsk, Tobychan, Elga Miles, and Watson. Enrichment in W and Ga of IIE metal could result from self-reduction during the melting of the H chondrite parent body. The Os/Ir and Au/As correlations indicate a magmatic origin of the IIE metal. The distribution of 24 siderophile elements in the metal indicates that the IIE iron meteorites could be formed at the middle and late stages of fractional crystallization of a metallic melt of H chondrite initial composition—Verkhne Dnieprovsk ~40%, Tobychan ~45%, Watson ~55%, Elga ~70%, and Miles ≥73%. This geochemical evidence shows that the formation of the IIE metal is inconsistent with the crystallization of IIEs in a melt pool at the surface, or inside the core of a parent body. We propose a modified hybrid model based on multistage formation of the IIE meteorites: (1) accretion of an H chondritic-like initial parent body and its incomplete internal differentiation with the formation of a metal core and silicate mantle with the preservation of the external chondritic layer; (2) impact events resulting in partial destruction of the IIE iron asteroid with the exposure of part of the core; (3) melting of the core material and mixing with chondritic material as a result of further impact events, followed by crystallization and post-magmatic changes in the structure of the metal and silicate inclusions. The proposed model successfully explains both textural and geochemical properties of the IIE metal and silicate components.

Acknowledgments—This article is dedicated to the memory of John Wasson for his pioneering contributions to the chemical study of metals in meteorites and his enduring interest in the origin of the IIE irons. We thank the editor, A. J. T. Jull, and reviewer, A.E. Rubin, for their detailed reviews, which greatly improved the paper. This work was supported by the Russian Foundation for Basic Research No. 20-05-00117 and research theme of the Vernadsky Institute No. 0137-2019-0002. Partial financial support was provided by the National Aeronautics and Space Administration Emerging Worlds program (80NSSC 18K0595). A portion of this work was performed at the National High Magnetic Field Laboratory, which is supported by the National Science Foundation Cooperative Agreement No. DMR-1644779 and the state of Florida.

Data Availability Statement—The data that support the findings of this study are available on request from the corresponding author. The data are not publicly available due to privacy or ethical restrictions.

Editorial Handling—Dr. A. J. Timothy Jull

REFERENCES

Abrahams, J. N. H., and Nimmo, F. 2019. Ferrovolcanism: Iron Volcanism on Metallic Asteroids. *Geophysical Research Letters* 46: 5055–64.

Anders, E., and Grevesse, N. 1989. Abundances of the Elements: Meteoritic and Solar. *Geochimica et Cosmochimica Acta* 53: 197–214.

Benedix, G. K., McCoy, T. J., Keil, K., and Love, S. G. 2000. A Petrologic Study of the IAB Iron Meteorites: Constraints on the Formation of the IAB-Winonaite Parent Body. *Meteoritics & Planetary Science* 35: 1127–41.

Bevan, A. W. R., Kinder, J., and Axon, H. J. 1979. A Metallographic Study of the Iron Meteorite Verkhne Dnieprovsk (BM 51183). *Mineralogical Magazine* 43: 149–54.

Bild, R. W., and Wasson, J. T. 1977. Netschaevo: A New Class of Chondritic Meteorite. *Science* 197: 58–62.

Birck, J. L., and Allègre, C. J. 1978. Chronology and Chemical History of the Parent Body of Basaltic Achondrites Studied by the ^{87}Rb-^{87}Sr Method. *Earth & Planetary Science Letter* 39: 37–51.

Bishop, M. C., Moynier, F., Wenstein, C., Fraboulet, J.-G., Wang, K., and Foriel, J. 2012. The Cu Isotopic Composition of Iron Meteorites. *Meteoritics & Planetary Science* 47: 268–76.

Buchwald, V. F. 1976. Handbook of iron meteorites. In *Their History, Distribution, Composition and Structure* Berkeley and London: Univ. of California Press, xii + 1426 pp. 2124 figs (3 volumes).

Buchwald, V. F., and Clarke, R. S. 1987. The Verkhne Dnieprovk Iron Meteorite Specimens in the Vienna Collection and the Confusion of Verkhne Dnieprovk with Augustinovka. *Meteoritics* 22: 121–35.

Burkhardt, C., Kleine, T., Oberli, F., Pack, A., Bourdon, B., and Wieler, R. 2011. Molybdenum Isotope Anomalies in Meteorite: Constraints on Solar Nebula Evolution and Origin of the Earth. *Earth & Planetary Science Letters* 312: 390–400.

Campbell, A. J., and Humayun, M. 1999. Trace Element Microanalysis in Iron Meteorites by Laser Ablation ICPMS. *Analytical Chemistry* 71: 939–46.

Campbell, A. J., and Humayun, M. 2005. Compositions of Group IVB Iron Meteorites and Their Parent Melt. *Geochimica et Cosmochimica Acta* 69: 4733–44.

Campbell, A. J., Humayun, M., and Weisberg, M. K. 2002. Siderophile Element Constraints on the Formation of Metal in the Metal-Rich Chondrites Bencubbin, Weatherford, and Gujba. *Geochimica et Cosmochimica Acta* 66: 647–60.

Casanova, L., Graf, T., and Marti, K. 1995. Discovery of an Unmelted H Chondrite Inclusion in an Iron Meteorite. *Science* 268: 540–2.

Chabot, N. L., Campbell, A. J., Jones, J. H., Humayun, M., and Agee, C. B. 2003. An Experimental Test of Henry's Law in Solid Metal Liquid Metal Systems with Implications for Iron Meteorites. *Meteoritics & Planetary Science* 38: 181–96.

Chabot, N. L., and Jones, J. H. 2003. The Parameterization of Solid Metal-Liquid Metal Partitioning of Siderophile Elements. *Meteoritics & Planetary Science* 38: 1425–36.

Chabot, N. L., Saslow, S. A., McDonough, W. F., and Jones, J. H. 2009. An Investigation of the Behavior of Cu and Cr During Iron Meteorite Crystallization. *Meteoritics & Planetary Science* 44: 505–19.

Clayton, R. N., and Mayeda, T. K. 1996. Oxygen Isotope Studies of Achondrites. *Geochimica et Cosmochimica Acta* 60: 1999–2018.

Corrigan, C. M., Chabot, N. L., McCoy, T. J., McDonough, W. F., Watson, H. C., Saslow, S. A., and Ash, R. D. 2009. The Iron-Nickel Phosphorus System: Effects on the Distribution of Trace Elements During the Evolution of Iron Meteorites. *Geochimica et Cosmochimica Acta* 73: 2674–91.

Ebihara, M., Ikeda, Y., and Prinz, M. 1997. Petrology and Chemistry of the Miles IIE Iron II: Chemical Characteristics of the Miles Silicate Inclusions. *Antarctic Meteorite Research* 10: 373–88.

Fischer-Godde, M., Becker, H., and Wombacher, F. R. 2010. Rhodium, Gold and Other Highly Siderophile Element Abundances in Chondritic Meteorites. *Geochimica et Cosmochimica Acta* 74: 356–79.

Gaboardi, M., and Humayun, M. 2009. Elemental Fractionation During LA-ICP-MS Analysis of Silicate Glasses: Implications for Matrix-Independent Standardization. *Journal of Analytical Atomic Spectrometry* 24: 1188–97.

Gaffey, M. J., and Gilbert, S. L. 1998. Asteroid 6 Hebe: The Probable Parent Body of the H-Type Ordinary Chondrites and the IIE Iron Meteorites. *Meteoritics & Planetary Science* 33: 1281–95.

Humayun, M. 2012. Chondrule Cooling Rates Inferred from Diffusive Profiles in Metal Lumps from the Acfer 097 CR2 Chondrite. *Meteoritics & Planetary Science* 47: 1191–208.

Hunt, A. C., Cook, D. L., Lichtenberg, T., Reger, P. M., Ek, M., Golabeck, G. J., and Schoenbaechler, M. 2018. Late Metal-Silicate Separation on the IAB Parent Asteroid: Constraints from Combined W and Pt Isotopes and Thermal Modelling. *Earth and Planetary Science Letters* 482: 490–500.

Ikeda, Y., Ebihara, M., and Prinz, M. 1997. Petrology and Chemistry of the Miles IIE Iron. Description and Petrology of Twenty New Silicate Inclusions. *Antarctic Meteorite Research* 10: 355–72.

Ikeda, Y., and Prinz, M. 1996. Petrology of Silicate Inclusions in the Miles IIE Iron Proceedings NIPR Symposium. *Antarctic Meteorites* 9: 143–73.

Jarosewich, E. 1990. Chemical Analyses of Meteorite: A Compilation of Stony and Iron Meteorite Analyses. *Meteoritics* 25: 323–37.

Jochum, K. P., Stoll, B., Herwig, K., Willbold, M., Hofmann, A. W., Amini, M., Aarburg, S., et al. 2006. MPI-DING Reference Glasses for In Situ Microanalysis: New Reference Values for Element Concentrations and Isotope Ratios. *Geochemistry, Geophysics, Geosystem* 7: 1–44.

Jones, J. H., and Drake, M. J. 1983. Experimental Investigations of Trace Element Fractionation in Iron Meteorites, II: The Influence of Sulfur. *Geochimica et Cosmochimica Acta* 47: 1199–209.

Jones, J. H., and Malvin, D. J. 1990. A Nonmetal Interaction Model for the Segregation of Trace Metals During Solidification of Fe-Ni-S, Fe-Ni-P, and Fe-Ni-S-P Alloys. *Metallurgical and Materials Transactions* B21: 697–706.

Khisina, N. R., Abdrakhimov, A. M., and Wirth, R. 2019. Liquid Immiscibility in Regions of Localized Shock-Induced Melting in the Elga Meteorite. *Geochemica International* 57: 903–11.

Khisina, N. R., Teplyakova, S. N., Wirth, R., Senin, V. G., Averin, A. A., and Shiryaev, A. A. 2017. Carbon-Bearing Phases in Shock-Induced Melt Zones of the Elga Meteorite. *Geochemica International* 55: 317–29.

Kong, P., and Ebihara, M. 1997. The Origin and Nebular History of the Metal Phase of Ordinary Chondrites. *Geochimica et Cosmochimica Acta* 61: 2517–29.

Kruijer, T. S., and Kleine, T. 2019. Age and Origin of IIE Iron Meteorites Inferred from Hf-W Chronology. *Geochimica et Cosmochimica Acta* 262: 92–103.

Litasov, K. D., Teplyakova, S. N., Shatskiy, A., and Kuper, K. E. 2019. Fe-Ni-P-S Melt Pockets in Elga IIE Iron Meteorite: Evidence for the Origin at High-Pressures up to 20 GPa. *Minerals* 9: 616.

Luais, B. 2007. Isotopic Fractionation of Germanium in Iron Meteorites: Significance for Nebular Condensation, Core Formation and Impact Processes. *Earth and Planetary Science Letters* 262: 21–36.

Markowski, A., Quitter, G., Halliday, A. N., and Kleine, T. 2006. Tungsten Isotopic Compositions of Iron Meteorites: Chronological Constraints vs. Cosmogenic Effects. *Earth and Planetary Science Letters* 242: 1–15.

Maurel, C., Bryson, J. F. J., Shah, J., Chopdekar, R. V., Elkins-Tanton, L. T., Raymond, C. A., and Weiss, B. P. 2021. A Long-Lived Planetesimal Dynamo Powered by Core Crystallization. *Geophysical Research Letters* 48: e2020GL091917. https://doi.org/10.1029/2020GL091917.

McCoy, T. J. 1995. Silicate-Bearing IIE Irons: Early Mixing and Differentiation in a Core–Mantle Environment and Shock Resetting of Ages. *Meteoritics* 30: 542–3.

McCoy, T. J. 2011. Group IVA Irons: New Constraints on the Crystallization and Cooling History of an Asteroidal Core with a Complex History. *Geochimica et Cosmochimica Acta* 75: 6821–43.

McDermott, K. H., Greenwood, R. C., Scott, E. R. D., Franchi, I. A., and Anand, M. 2016. Oxygen Isotope and Petrological Study of Silicate Inclusions in IIE Iron Meteorites and Their Relationship with H Chondrites. *Geochimica et Cosmochimica Acta* 173: 97–113.

Meteoritical Bulletin Database. 2022. Retrieved from https://www.lpi.usra.edu/meteor/

Mittlefehldt, D., McCoy, T., Goodrich, C., and Kracher, A. 1998. Non-Chondritic Meteorites from Asteroidal Bodies. In *Planetary Materials*, edited by J. J. Papike, 4-1–4-195. Washington, DC: Mineralogical Society of America.

Olsen, E., Davis, A., Clarke, R. J., Jr., Schultz, L., and Weber, H. W. 1994. Watson: A New Link in the IIE Iron Chain. *Meteoritics* 29: 200–13.

Osadchii, E. G., Baryshnikova, G. V., and Novikov G. V. 1981. The Elga Meteorite: Silicate Inclusion and Shock Metamorphism. Proceedings, 12th Lunar and Planetary Science Conference. pp. 1049–68.

Prinz, Z. M., Nehru, C. E., Delaney, J. S., Harlow, G. E., and Bedell, R. L. 1980. Modal Studies of Mesosiderites and Related Achondrites, Including the New Mesosiderite ALHA77219. Proceedings, 11th Lunar and Planetary Science Conference. pp. 1055–71.

Qin, L., Dauphas, N., Wadhwa, M., Masarik, J., and Janney, P. E. 2008. Rapid Accretion and Differentiation of Iron Meteorite Parent Bodies Inferred from ^{182}Hf–^{182}W Chronometry and Thermal Modeling. *Earth & Planetary Science Letters* 273: 94–104.

Raghavan, V. 1988. The Fe–Ni–P (Iron–Nickel–Phosphorus) System. *Phase Diagrams Ternary Iron Alloys* 3: 121–37.

Rubin, A. 2022. IIE Irons: Origin, Relationship to Ordinary Chondrites, and Evidence for Siderophile-Element Fractionations Caused by Chondrule Formation. *Meteoritics and Planetary Science* 57: 163–84. https://doi.org/10.1111/maps.13693.

Russell, S. S., McCoy, T. J., Jarosewich, E., and Ash, R. D. 1998. The Burnwell, Kentucky, Low Iron Chondrite Fall: Description, Classification and Origin. *Meteoritics & Planetary Science* 33: 853–6.

Ruzicka, A. 2014. Silicate-Bearing Iron Meteorites and Their Implications for the Evolution of Asteroidal Parent Bodies. *Chemie der Erde* 74: 3–48.

Ruzicka, A., Fowler, G. W., Snyder, G. A., Prinz, M., Papike, J. J., and Taylor, L. A. 1999. Petrogenesis of Silicate Inclusions in the Weekeroo Station IIE Iron Meterorite: Differentiation, Remelting and Dynamic Mixing. *Geochimica et Cosmochimica Acta* 63: 2123–43.

Ruzicka, A., and Hutson, M. 2010. Comparative Petrology of Silicates in the Udei Station (IAB) and Miles (IIE) Iron Meteorites: Implications for the Origin of Silicate-Bearing Irons. *Geochimica et Cosmochimica Acta* 74: 394–433.

Scherstén, A., Elliott, T., Hawkesworth, C., Russell, S., and Masarik, J. 2006. Hf–W Evidence for Rapid Differentiation of Iron Meteorite Parent Bodies. *Earth & Planetary Science Letters* 241: 530–42.

Schmitt, W., Palme, H., and Wanke, H. 1989. Experimental Determination of Metal/Silicate Partition Coefficients for P, Co, Ni, Cu, Ga, Ge and W and Some Implications for the Early Evolution of the Earth. *Geochimica et Cosmochimica Acta* 53: 173–85.

Schulz, T., Munker, C., Palme, H., and Mezger, K. 2009. Hf–W Chronometry of the IAB Iron Meteorite Parent Body. *Geochimica et Cosmochimica Acta* 280: 185–93.

Schulz, T., Upadhyay, D., Munker, C., and Mezger, K. 2012. Formation and Exposure History of Non-Magmatic Iron Meteorites and Winonaites: Clues from Sm and W Isotopes. *Geochimica et Cosmochimica Acta* 85: 200–12.

Scott, E. R. D., and Wasson, J. T. 1976. Chemical Classification of Iron Meteorites. VIII. Groups IC, IIE, IIIF and 97 Other Irons. *Geochimica et Cosmochimica Acta* 40: 103–15.

Scott, E. R. D., Wasson, J. T., and Buchwald, V. F. 1973. The Chemical Classification of Iron Meteorites VII. A Reinvestigation of Irons with E Concentrations Between 25 and 80 ppm. *Geochimica et Cosmochimica Acta* 37: 1957–83.

Snyder, G. A., Lee, D.-C., Ruzicka, A. M., Prinz, M., Taylor, L. A., and Halliday, A. N. 2001. Hf–W, Sm–Nd, and Rb–Sr Isotopic Evidence of Late Impact Fractionation and Mixing of Silicates on Iron Meteorite Parent Bodies. *Earth & Planetary Science Letters* 186: 311–24.

Srinivasan, G., Whitehouse, M. J., Weber, I., and Yamaguchi, A. 2006. Crystallization Ages of Zircons on Eucrite Parent Body from Hf-W Systematics (Abstract #2042). 37th Lunar and Planetary Science Conference. CD-ROM.

Teplyakova, S. N., Humayun, M., Lorenz, C. A., and Ivanova, M. A. 2012. A Common Parent for IIE Iron Meteorites and H Chondrites (Abstract #1130). 43rd Lunar and Planetary Science Conference. CD-ROM.

Teplyakova, S. N., and Lorenz, C. A. 2019. Metal Crystallization in IIE Irons and Their Possible Meteorite Analogues. *Geochemistry International* 57: 893–902.

Teplyakova, S. N., Lorenz, C. A., Ivanova, M. A., Kononkova, N. N., Anosova, M. O., Ryazantsev, K. M., and Kostitsyn, Y. A. 2018. Mineralogy of Silicate Inclusions in the Elga IIE Iron Meteorite. *Geochemistry International* 56: 1–23.

Troiano, J., Rumble, D., Rivers, M. L., and Friedrich, J. M. 2011. Compositions of Three Low-FeO Ordinary Chondrites: Indications of a Common Origin with the H Chondrites. *Geochimica et Cosmochimica Acta* 75: 6511–9.

Van Roosbroek, N., Hamann, C., McKibbin, S., Greshake, A., Wirth, R., Pittarello, L., Hecht, L., Claeys, P., and Debaille, V. 2017. Immiscible Silicate Liquids and Phosphoran Olivine in Netscaevo IIE Silicate: Analogue for Planetesimal Core–Mantle Boundaries. *Geochimica et Cosmochimica Acta* 197: 378–95.

Walker, R. J., McDonough, W. F., Honesto, J., Chabot, N. L., McCoy, T. J., Ash, R. D., and Bellucci, J. J. 2008. Modeling Fractional Crystallization of Group IVB Iron Meteorites. *Geochimica et Cosmochimica Acta* 72: 2198–216.

Wasserburg, G. J., Sanz, H. G., and Bence, A. E. 1968. Potassium Feldspar Phenocrysts in the Surface of Colomera, and Iron Meteorite. *Science* 161: 684–7.

Wasson, J. T. 1999. Trapped Melt in IIIAB Irons: Solid/Liquid Elemental Partitioning During the Fractionation of the IIIAB Magma. *Geochimica et Cosmochimica Acta* 63: 2875–89.

Wasson, J. T. 2017. Formation of Non-Magmatic Iron-Meteorite Group IIE. *Geochimica et Cosmochimica Acta* 53: 396–416.

Wasson, J. T., Huber, H., and Malvin, D. J. 2007. Formation of IIAB Iron Meteorites. *Geochimica et Cosmochimica Acta* 71: 760–81.

Wasson, J. T., and Kallemeyn, G. W. 1988. Composition of Chondrites. *Philosophical Transactions of the Royal Society A* 328: 535–44.

Wasson, J. T., Ouyang, X., Wang, J., and Jerde, E. 1989. Chemical Classification of Iron Meteorites: XI. Multi-Element Studies of 38 New Irons and the High Abundance of Ungrouped Irons from Antarctica. *Geochimica et Cosmochimica Acta* 53: 735–44.

Wasson, J. T., and Richardson, J. W. 2001. Fractionation Trends Among IVA Iron Meteorites: Contrasts with IIIAB Trends. *Geochimica et Cosmochimica Acta* 65: 951–70.

Wasson, J. T., and Scott, E. R. D. 2011. Group II Iron Meteorites; Metal Composition, Formation, Relationship to Ordinary Chondrites (Abstract # 2813). 42nd Lunar and Planetary Science Conference. CD-ROM.

Wasson, J. T., and Wang, J. 1986. A Nonmagmatic Origin of Group-IIE Iron Meteorites. *Geochimica et Cosmochimica Acta* 50: 725–32.

Willis, J., and Goldstein, J. I. 1982. The Effects of C, P, and S on Trace Element Partitioning During Solidification in Fe-Ni Alloys. *Proceedings of Lunar Planetary Science Conference, Part I. Journal of Geophysics Research* 87: A435–45.